ORIGINAL ARTICLE

Verifying antibacterial properties of nanopillars on cicada wings

Richard W. van Nieuwenhoven[1] · Alexander M. Bürger[1] · Laura L. E. Mears[1] · Philip Kienzl[2] · Manuel Reithofer[3] ·
Adelheid Elbe-Bürger[2] · Ille C. Gebeshuber[1]

© The Author(s) 2024

Abstract

The antibacterial properties of cicada wings originate from hexagonally arranged pillar-like multi-functional nanostructures with species-dependent heights, which are super-hydrophobic and self-cleaning. In the present study, two cicada species with promising nanopillars were investigated in more detail. Selected methods were used to analyze the wing surfaces, including Atomic Force Microscopy, Scanning Electron Microscopy, and bacterial tests with live/dead staining. Verifying the antibacterial properties posed challenges, such as the bacteria concentration needed to confirm the antibacterial properties. These challenges will also impact the practical implementation of antibacterial nanostructures and support the findings of recent critical publications.

Keywords Antibacterial · Cicada wings · Nanopillar · Superhydrophobicity · Biomimetics · Bioinspired

Introduction

Elena P. Ivanova and co-workers (Ivanova et al. 2012) reported about cicada wing antibacterial properties based on the surface nanopillars in 2012. Various studies followed this lead, spreading the field to different insect species on the one hand and multiple methods of surface nanopillar reproduction on the other hand (Ivanova et al. 2012, 2013a, b, 2017; Hasan et al. 2012; Kelleher et al. 2015; Román-Kustas et al. 2020; Pogodin et al. 2013; Tripathy et al. 2017; Bandara et al. 2017). Especially medical devices would benefit from the antibacterial properties based on the nanostructured surfaces by inherently inhibiting bacterial colonization.

The three suggested physical antibacterial mechanisms of nanopillar-covered surfaces start with adherence of the bacterial membrane (BM) to the tips of the nanopillars. The adhesive forces between the BM and the nanopillar sides pull the BM down along the nanopillar sides between the nanopillars. The BM surface gets overstretched, causing the tip to penetrate the bacteria, or the BM spanning the area between the nanopillars loses integrity (Román-Kustas et al. 2020; Ivanova et al. 2012, 2017; Pogodin et al. 2013). Alternatively, displacements of the bacteria after adhering to the top of the nanopillars can tear open the BM, particularly when the height of the nanopillars fluctuates (Román-Kustas et al. 2020).

The present study reports about the nanopillar wing topology of two New Zealand cicada species *Amphipsalta cingulata* and *Kikihia scutellaris*, with especially *K.scutellaris* showing promising results regarding nanopillar-based antibacterial properties of the wing surface. This study included the development of a photopolymer resin replica based on

✉ Richard W. van Nieuwenhoven
nieuwenhoven@iap.tuwien.ac.at

Alexander M. Bürger
alexander.buerger@tuwien.ac.at

Laura L. E. Mears
mears@iap.tuwien.ac.at

Philip Kienzl
philip.kienzl@meduniwien.ac.at

Manuel Reithofer
manuel.reithofer@boku.ac.at

Adelheid Elbe-Bürger
adelheid.elbe-buerger@meduniwien.ac.at

Ille C. Gebeshuber
gebeshuber@iap.tuwien.ac.at

[1] Institute of Applied Physics, TU Wien, Wiedner Hauptstraße 8-10, 1040 Vienna, Austria

[2] Department of Dermatology, Medical University of Vienna, Währinger Gürtel 18-20, 1090 Vienna, Austria

[3] Institute of Molecular Biotechnology, University of Natural Resources and Life Sciences Vienna, Muthgasse 18, 1190 Vienna, Austria

Springer

previous studies utilising polyvinyl siloxane (PVS) (Bürger 2022; van Nieuwenhoven 2022; Koch et al. 2008; Zobl 2018).

In the referenced previous studies, many different protocols were followed to show the antibacterial properties. In the absence of standardized antibacterial surface testing protocols, this study describes a fine-grained protocol on how the antibacterial properties were verified (Bürger 2022; van Nieuwenhoven 2022).

The antibacterial properties of the nanostructures were demonstrated using the designated protocols. The nanopillars on the previously undocumented cicada species *A. cingulata* and *K. scutellaris* present an impediment to the adherence of bacteria to the nanopillars. Based on the verification results, we created a hypothesis on the efficiency of the antibacterial properties of the nanostructures on cicada wings.

Materials and methods

Samples of the two cicada species for this study, namely the lesser bronze cicada *Kikihia scutellaris* (Fig. 1a) and the clapping cicada *Amphipsalta cingulata* (Fig. 1b), were collected in a dead state in New Zealand (Baracchi and Baciadonna 2020).

Both New Zealand cicadas selected for the study have nanopillars. We focused the replication on *K. scutellaris* due to higher nanopillars ("Wing topology analysis section) and abundant availability. Employing casting and curing of PVS at 4°C enabled the creation of cicada wing surface replicas

with nanoscale precision (Bürger 2022; van Nieuwenhoven 2022; Koch et al. 2008; Zobl 2018).

Preparation

The wings were carefully removed from the thorax and used without any further cleaning steps. A window-like rigid vein structure supports the membrane of the cicada wings. The more prominent veins (due to their thickness and aspect ratio) reduce the nanopillar-covered area and the field of view, especially during microscopy. A biopsy punch (Kai Medical Biopsy Punch 5 mm, Kai Industries Co. Ltd., Seki, Japan) was used to cut comparable 5 mm discs out of the wings. The more prominent veins were excluded during sectioning.

Atomic force microscopy

An atomic force microscope (AFM) was used in tapping mode to minimize destructive interactions of the AFM tip with the sample.

Most AFM investigations were performed with an MFP-3D-BIO AFM (Asylum Research, Oxford Instruments plc) because the more accessible chamber enables a faster switching time between different samples. However, some investigations used the Cypher ES (Asylum Research, Oxford Instruments plc, Abingdon, United Kingdom) Atomic Force Microscope (AFM). The tips used in all scans were BudgetSensors® Tap300-G (resonance frequency 300 kHz; force constant 40 N/m, the cantilever was made of uncoated monolithic Silicon).

Fig. 1 Both cicada species for this study are endemic to New Zealand and were collected in a dead state. © 2021, Alexander M. Bürger. Scale bar is 1 cm. **a** *Kikihia scutellaris*, the lesser bronze cicada. **b** *Amphipsalta cingulata*, the clapping cicada

Scanning electron microscopy

The Scanning Electron Microscopy (SEM) micrographs used in this research were taken with a Scios 2 DualBeam and an FEI Quanta 250 FEG (from Thermo Fisher Scientific GmbH, Waltham, Massachusetts, U.S.) at the University Service Centre for Transmission Electron Microscopy, Vienna University of Technology, Austria. The cicada wings were washed in distilled water ultrasonic bath for 10 min and afterward put under a stream of nitrogen to remove the water residuals. In addition, the wings of both species with attached *E. coli* bacteria were studied by air-drying the wings after immersing them in a bacterial suspension $OD^{600} = 0.7$ for one hour. All samples were mounted using double-sided adhesive carbon tape (Thermo Fisher Scientific GmbH, Waltham, Massachusetts, U.S.) and sputtered with a 4 nm gold/palladium layer.

Bacterial testing

Testing protocols for analyzing the efficiency of antibacterial nanostructured surfaces are not readily available, and previous studies used diverse techniques and protocols to show the antibacterial properties (Ivanova et al. 2012, 2013a, b, 2017; Hasan et al. 2012; Kelleher et al. 2015; Román-Kustas et al. 2020; Pogodin et al. 2013; Tripathy et al. 2017; Bandara et al. 2017). The testing protocol of this study was designed based on the experiences of these previous studies.

For the antibacterial tests, as representative of Gram-negative bacteria *Escherichia coli* (*E. coli*, DSM 5698/ATCC 25404) and as representative of Gram-positive bacteria *Staphylococcus aureus* (*S. aureus*, DSM 1104/ATCC 25923) were used, both obtained from the Leibnitz Institute (DSMZ-German Collection of Microorganisms and Cell Culture GmbH, Braunschweig, Germany).

The initial cultivation was performed in Lysogeny broth (LB-medium), which was produced after the standard protocol developed by Giuseppe Bertani Bertani (1951). Stock bacteria solutions were mixed in a 1:1 ratio with a 50% glycerol solution in phosphate-buffered saline (PBS, Life Technologies Limited, United Kingdom). The suspension was mixed at 800 rpm in a thermal shaker (Thermomixer Compact 5350, Eppendorf SE, Hamburg, Germany) before distributing 1 ml per Eppendorf tube® (Eppendorf SE, Hamburg, Germany) and stored at $-50\,°C$.

Before each experiment, the bacteria were gradually thawed and suspended in LB medium and mixed at 800 rpm in the thermal shaker at 37 °C.

The bacteria concentration was determined by measurement of the optical density (OD^{600}) at wavelength 600 nm with a BioTek EL800 plate reader (The Lab World Group, Hudson, MA, U.S.). The bacteria were grown until they reached an optical density of OD^{600} of 0.7. An OD^{600} of

0.7 is commonly used in studies on antibacterial properties (Sambrook and Russell 2001) as the bacterial growth is at its optimum at the end of the exponential growth phase (Hall et al. 2013; Buchanan 1918). Former studies on the antibacterial properties of cicada wings used OD^{600} in the range of 0.1 and 0.3 (Hasan et al. 2012; Kelleher et al. 2015; Román-Kustas et al. 2020). This study stayed with the OD^{600} value of 0.7 from the laboratory manual (Sambrook and Russell 2001).

Bacteria fluorescence stains

Live/dead staining was performed with propidium iodide (PI) (Sigma-Aldrich, Merck SA, Germany) and bisbenzimide Hoechst 33343 (Hoechst) (Sigma-Aldrich, Merck SA, Germany) fluorescence stains. PI is a nucleic acid stain that does not permeate intact membranes and stains only dead cells with damaged membranes. In comparison, Hoechst is a DNA stain that can pass intact cell membranes. The PI was dissolved in distilled water to a stock concentration of 1 mg/ml. During experiments, the concentration of the stock solution was further reduced with PBS to 40 µl/ml (Ciancio et al. 1988; Scientific 2021). Hoechst was dissolved in distilled water to a stock concentration of 0.5 mg/ml. Methanol-based fixation(Mangels et al. 1984) was done by adding 25% methanol to the Hoechst staining solution. Experimental concentration was reached by dissolving the stock solution in a PBS/methanol mixture (75/25) to 6 µl/ml (Ciancio et al. 1988; Scientific 2021).

Testing protocol

Five-millimeter diameter samples (cicada wing, 3D-printed disks) were glued into 3D-printed bottomless wells with nail polish onto a microscope slide. All 3D-printed parts were printed using photopolymer resin (Elegoo ABS-Like LCD UV photopolymer rapid resin, GE-EL-3D-005, Elegoo, Shenzhen, China) with an Elegoo Mars and a Phrozen Sonic Mini 8K. The sample was incubated in the well for one hour with 350 µl bacterial suspension at room temperature. Blank poly-L-lysine coated microscope slides (Electron Microscopy Sciences, Hatfield, Pennsylvania, U.S.) were used as a control group for the cicada wings. The empty well was directly glued to the slide for these coated slides. To exclude the potentially toxic effects of the used resin residues on the viability of bacteria, a 3D-printed 5 mm diameter disk with $100x40x40\,\mu m^3$ pillars was used as a control specimen. Such large pillars do not have any mechanical effect on the bacteria.

In the first staining step, 110 µl of the PI/PBS solution was pipetted in each well after gradually extracting the bacteria suspension and incubating for 15 min. For

the dead control group, 25% of the PBS from this step was replaced by methanol. The samples were protected from light during the whole staining procedure. Afterwards, the samples were gently washed with 110 µ PBS to remove unbound PI stain and unattached bacteria. The samples were exposed to 110 µl Hoechst/PBS/methanol for 30 min, again shielded from light. Then the suspension and the surrounding well were removed from the microscope slide, leaving the sample glued in the center. Fluoromount-G™(00-4958-02, Thermo Fisher Scientific GmbH, Waltham, Massachusetts, U.S.) was applied to the sample with a cover slip to enhance the stability of the fluorescence stains (PI/Hoechst). The margin of the cover slip was sealed with nail polish to prevent the evaporation of the Fluoromount-G™.

The fluorescence imaging of the wings was performed with an IX73 inverted microscope (Olympus Corporation, Tokyo, Japan) at the Department of Dermatology and a Zeiss LSM 880 Airyscan (Carl Zeiss AG, Oberkochen, Germany) at the Core Facility Imaging, both at the Medical University of Vienna. PI was excited at 561 nm, and the emission was measured at 640 nm, whereas Hoechst was excited at 405 nm and measured at 488 nm.

The fluorescence image color channels were analyzed separately with the software Fiji Schindelin et al. (2012). In the bright field channel of the image, clusters could be separated into single bacteria.

Bacteria counting in the two micrometer above the nanopillars

At the end of the 60-min incubation cycle and just before the staining started, 20 µl of the bacteria-containing fluid was slowly (with as little disturbance of the solution as possible) extracted from the bottom of the container with a pipette. The concentration of the droplet collected from the bottom also represents the concentration of the 2 µm above the nanopillars. The 20 µl droplet was transferred to a 15×15 mm^2 cover slip.

Subsequently, a second cover slip was positioned on top of the droplet. The droplet completely filled the area between the two cover slips without spilling. Brightfield images of the plain between the cover slips were obtained with a Zeiss LSM 880 Airyscan (Carl Zeiss AG, Oberkochen, Germany) and were used for counting the bacteria with Fiji Schindelin et al. (2012). The counting was done automatically using the Fiji built-in function "find maxim" after twice applying the Fiji-filter-maximum with a radius of 5 pixels and the Fiji FFT bandpass filter (between 40 and 3 pixels) to remove the background shading.

Contact angle

The hydrophobic properties of the cicada wing were investigated with a 3 µl deionized waterdrop pipetted on a veinless spot on the wing sample. The open-source software OpenDrop Huang et al. (2021) was used to analyze the contact angle in the images taken with a Thorlabs CMOS Camera (Thorlabs, Newton, New Jersey, U.S.) with a telecentric lens (0.5x, 65 mm WD CompactTL TM Telecentric Lense, Edmund Optics Inc., Barington, New Jersey, U.S.).

Results and discussion

Wing topology analysis

To analyse the antibacterial properties of the nanopillars on the cicada wing surface, we first need to characterise the topology. SEM micrographs of the *K. scutellaris* (Fig. 2a) and the *A. cingulata* (Fig. 2b) wing surface both show regular hexagonally structuring of nanopillars. In the zoom window, the rounded cone shape of the nanopillars can be observed.

The veins are rigid and thick (see Fig. 1a, b), and the membrane fabric is remarkably stable when comparing the wing to wings of other insects such as the common darter dragonfly. The height and center-to-center distance distribution of the nanopillars were also dependent on the position on the wing surface.

To thoroughly verify the location dependency of the height distribution, a more significant quantity of samples would be needed. The average nanopillar height fluctuated ±10% between AFM scans of the same species, and the center-to-center distance fluctuated ±3%. The data presented here were extracted from the most suitable AFM scans with the highest average nanopillars.

The regular structure can also be seen in the height distribution of the *A. cingulata* nanopillars (Fig. 4d). The nanopillars are, on average 251 nm high, with a σ of 29 nm. Because of the regular hexagonal positioning of the pillars, the distribution of the center-to-center distance has a low σ of 14 nm around a mean of 164 nm distance between the center of two nanopillars (Fig. 4c).

The nanopillar height on the wings of *K. scutellaris* was on average 241 nm with a σ of 42 nm (Fig. 4b). The center-to-center distance of the *K. scutellaris* nanopillars were on average 175 nm with a σ of 42 nm (Fig. 4a).

The cicada wing surface's hydrophobicity was verified by measuring the contact angle. *K. scutellaris* wing surface is on the border of superhydrophobicity, having a contact angle of 147° (Fig. 5a) whereas the *A. cingulata* showed a contact angle of 165° (Fig. 5b) and is clearly superhydrophobic; the
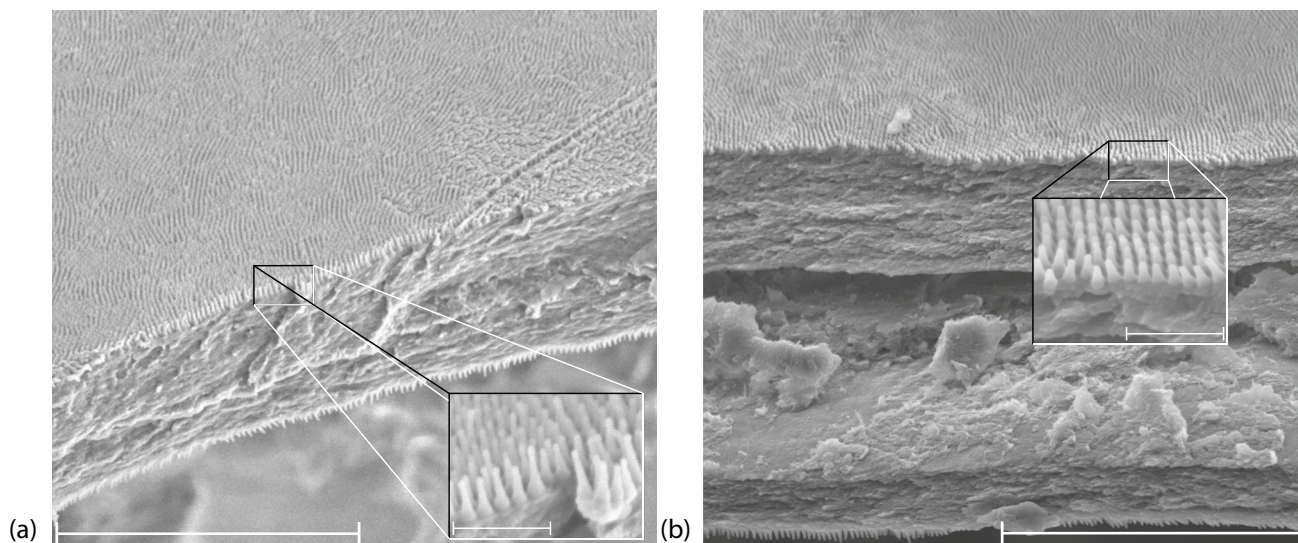
Fig. 2 Scanning electron micrographs (SEM) of cicada wing surfaces. **a** SEM micrograph of the *K. scutellaris* broken edge of the wing surface (scale bar 10 μm) with a detailed pillar view in the zoom window (scale bar 1 μm). **b** SEM micrograph from the broken edge of the *A. cingulata* wing surface (scale bar 10 μm) with a detailed pillar view in the zoom window (scale bar 1 μm)
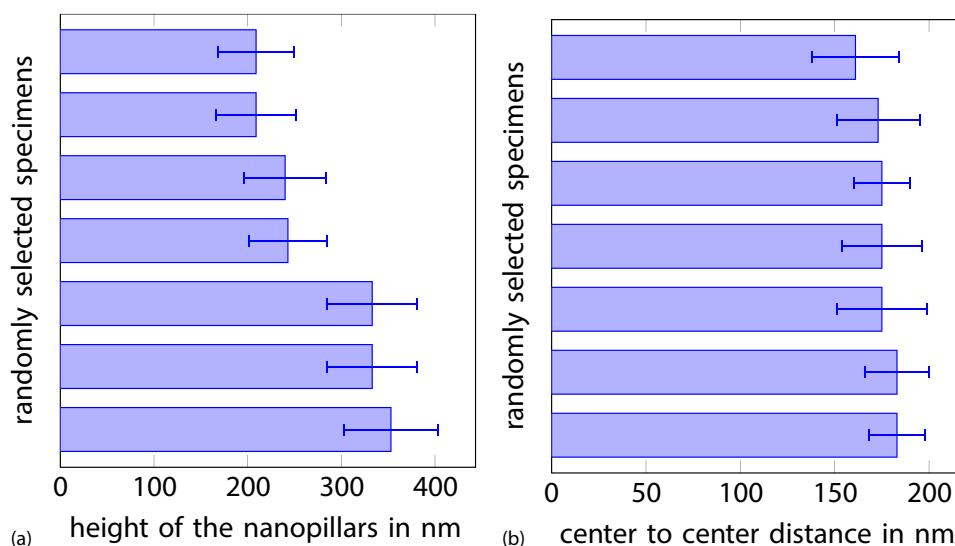
Fig. 3 Locational and individual differences of the nanopillars' height and center-center distance distributions for random *K. scutellaris* wing specimens. Multiple factors could be responsible for the height differences. The type of wing (hind or front wing), the specimen location on the wing, or even individual differences could cause these differences. **a** The height distribution of the nanopillars showed a clear specimen dependence. The highest pillar area measured on a specimen was 353 nm high with a σ of 50. **b** The differences in the center-to-center nanopillar distance measured on all specimens of the same species were in the margin of error from each other. The average center-to-center distance was 175 nm

limited available samples did not allow for a detailed investigation of the location dependency.

Antibacterial investigation

The live/dead test results show that the cicada wings of both species have antibacterial properties (Bürger 2022; van Nieuwenhoven 2022). Individual bacteria were counted in the Hoechst images (such as Fig. 6c), and the corresponding brightfield image (such as Fig. 6d) assists in the identification of individual bacteria in clusters. Cross-referencing the bacteria with PI images (such as Fig. 6a) identified the respective bacteria viability. Even though we are aware that more test results are needed for statistical evaluation of the

Fig. 4 Topological analysis of the nanostructures. The nanopillars on the wings of the *K. scutellaris* cicada were up to 100 nm higher (calculated from AFM scans with the respectively highest nanopillars, see Fig. 3b) than those of the *A. cingulata* cicada. **a** Histogram of *K. scutellaris* center-to-center nanopillar distance distribution with a mean of 174 nm, a textsigma of 24 nm and 707 counted nanopillars. **b** Histogram of *K. scutellaris* nanopillar height distribution with a mean of 353 nm, a textsigma of 50 nm and 707 counted nanopillars. **c** Histogram of *A. cingulata* center-to-center nanopillar distance distribution with a mean of 164 nm, a textsigma of 14 nm and 930 counted nanopillars. **d** Histogram of *A. cingulata* nanopillar height distribution with a mean of 251 nm, a textsigma of 29 nm and 930 counted nanopillars
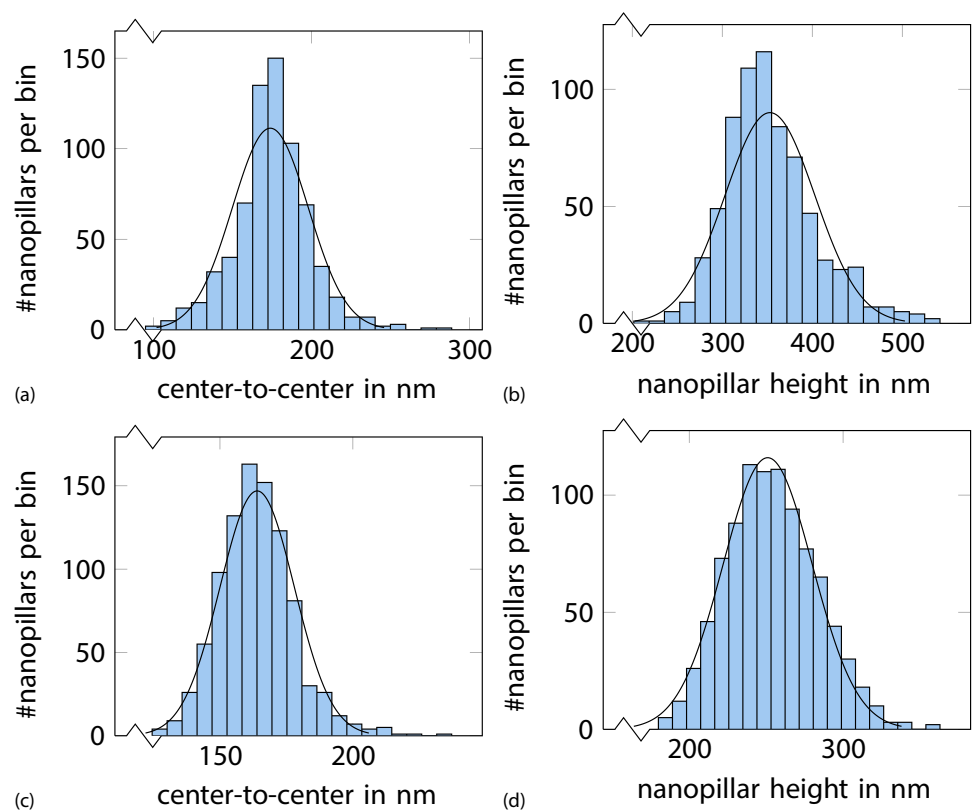
Fig. 5 The (super)hydrophobicity of the cicada wings was verified with contact angle measurements. **a** The 3 µl deionized waterdrop pipetted on a veinless spot on the *K. scutellaris* wing sample shows a contact angle of 147°. **b** The 3 µl deionized waterdrop pipetted on a veinless spot on the *A. cingulata* wing sample shows a contact angle of 165°
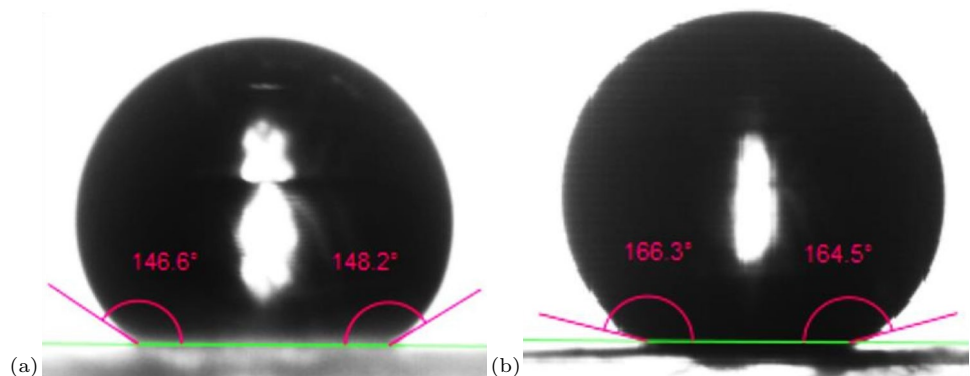
effectiveness, these results (Fig. 6b–d) show that the antibacterial properties (Fig. 6a) are present.

The verification of the antibacterial properties with this protocol ("Testing protocol" section) showed a discrepancy between the number of destroyed bacteria and the bacteria near the nanopillar surface ("Bacteria counting in the two micrometer above the nanopillars" section). The bacteria were adhering to the nanopillars at an low rate (see "Nanopillar attachments in context of bacteria concentration" section), and we hypothesize that the hydrophobicity is responsible for this behavior. In the course of this study, multiple critical publications about the antibacterial properties of nanostructured surfaces were published (Senevirathne et al. 2021; Michalska et al. 2021; Hawi et al. 2022; Valiei

et al. 2022). These studies also look into the superhydrophobic prohibition of bacteria attachment to nanopillars and the stacking bacteria on top of previously killed bacteria. The data these studies presented aligns with our hypothesis about the overall antibacterial efficiency. Recent mimetic studies are incorporating other antibacterial techniques into the nanopillar surface design, such as heat and reactive oxygen species (Zhang et al. 2021), to add multiple attack directions.

Nanopillar attachments in context of bacteria concentration

The bacteria solution was incubated directly on top of the nanopillar surface in all bacterial tests of this study. To

Fig. 6 Antibacterial investigation of the wing surface. **a** SEM micrograph of *E. coli* bacteria attached to the *K. scutellaris* nanopillars. Dead and living bacteria were identified with the Hoechst stain, whereas dead bacteria were identified with the PI stain. Confocal fluorescence LSM Image channels of the incubated *E. coli* bacteria on the *K. scutellaris*, combined scan $101 \times 101 \,\mu m^2$. **b** PI stained *E. coli* bacteria (red) in the PI image channel. **c** Hoechst stained *E. coli* bacteria (blue) in the Hoechst image channel. **d** The bright field reference channel was beneficial for separating colonies into single bacteria
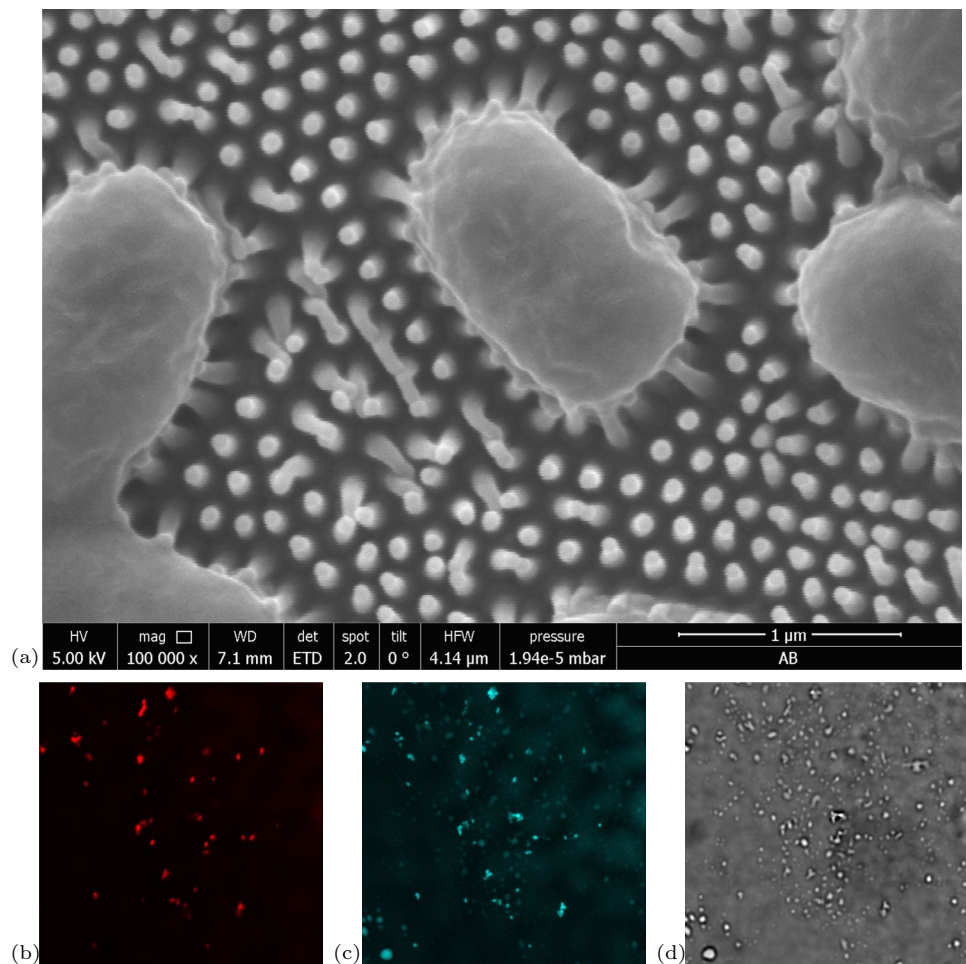
Fig. 7 Assessing the bacteria concentration during antibacterial tests. Brightfield image $(100 \times 100 \,\mu m^2)$ of *E. coli* bacteria extracted from near the wing surface, representing the two micrometers incubation medium above the nanopillars. **a** Initial image of the *E. coli* bacteria incubation medium concentration between the $15 \times 15 \, mm^2$ cover slips. **b** The same image (**a**), after applying the filters as specified in the counting ("Bacteria counting in the two micrometer above the nanopillars" section) protocol
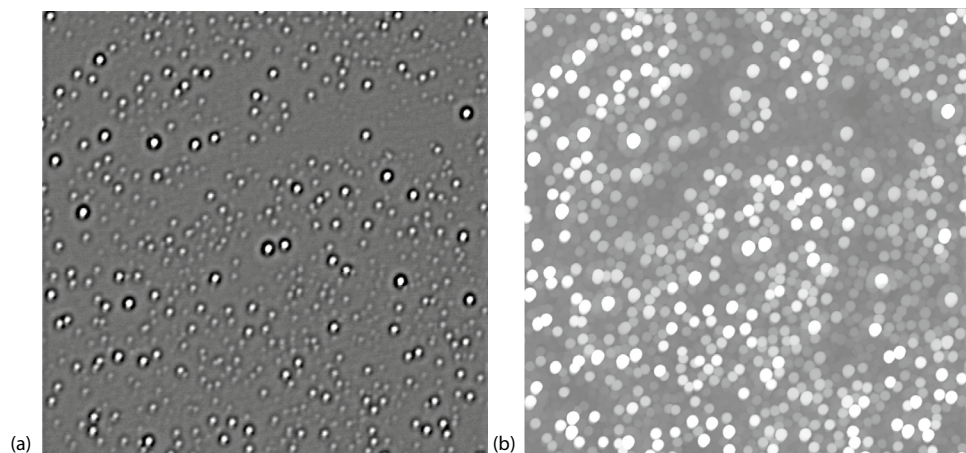
context, the number of attached bacteria to the number of bacteria in the two micrometres of the solution above the nanopillars and the concentration of the bacteria were evaluated. This section will focus on the calculations for the liquidation efficiency on *E. coli* bacteria, due to their inherent self-propulsion mechanisms, to open multiple ways

for determining the liquidation efficiency based on bacteria density $[L_e]$ and quantifying the nanopillar interactions $[L_{ea}]$.

Three random locations were selected for bacteria-counting images (Fig. 7) representing the volume from 0 to 2 µm above the nanopillars (with a total of 60,562 µm² imaged area). Applying the Fiji (Schindelin et al. 2012)

counting protocol above (see "Bacteria counting in the two micrometer above the nanopillars" section) results in 6621 counted bacteria. An estimation was made using the assumption of a homogeneous bacteria distribution of $\frac{15000\times15000}{60562} \times 6621 \approx 24.6 \times 10^6$ bacteria in the 15×15 mm^2 area between the two cover slips.

These experimental results indicate that 20 µl solution contains 24.6×10^6 bacteria. This counting method causes a disturbance in the layer of settled bacteria on the bottom of the incubation chamber, introduced by the pipette tip while entering the medium. The disturbance will remix some of the media and reduce bacteria concentration. Considering various possibilities of underestimating the absolute bacteria concentration $[B_c]$, $B_c = 1.2 \times 10^9$ bacteria per ml was used as a lower limit.

Using standard methods of calculating absolute bacteria concentrations from optical density, one can assume $B_c = 1 \times 10^9$ *E. coli* per ml. Other studies used calculations with an exponential curve (x = OD^{600}, y = # bacteria) $y = 5.8137 \times x^{0.9969} \times 0.9979$ (Zhang et al. 2015). This formula estimates 4×10^{11} bacteria in one ml at OD$^{600} = 0.7$. Therefore it can be estimated that one µl of *E. coli* medium at an OD^{600}=0.7 contains between $\frac{B_c}{1000} = 1 \times 10^6$ and $\frac{B_c}{1000} = 4 \times 10^8$ bacteria.

Our incubation container has a diameter of 7 mm and contains 350 µl of *E. coli* medium. Incubation is done in a resting environment so the bacteria will settle and concentrate at the bottom of the container. Especially *S. aureus* will settle and form colonies because they have no mechanical propulsion. The movement of *E. coli* will counter the settlement to a certain degree, but with the building of colonies, the movement will be reduced. The bottom of the well has a surface of 38.5×10^6 µm^2. In a perfect resting environment, the bottom can be covered by $\approx 2 \times 10^7$ packed bacteria (*E. coli* are approximately one by one by two µm^3 in volume).

Again assuming $B_c = 1 \times 10^9$ *E. coli* per ml, 350 µl, will contain at least 3.5×10^8 bacteria, which are enough bacteria in the solution to cover multiple layers with densely packed bacteria (In a perfectly settled environment). The nanopillars of the 100×100 µm^2 view window would be in continuous contact with $\approx 5 \times 10^3$ bacteria.

Alternatively, we evaluate the interaction frequency with the nanopillars of the self-propelling bacteria to estimate the liquidation efficiency. Therefore, we investigated the area of one to two bacteria diameters above the pillars. For *E. coli*, we select two micrometers. There is 2×10^4 µm^3 solution on top of the 100×100 µm^2 view window. Using the measured bacteria concentration of $B_c = 1.2 \times 10^9$ per ml, we can assume $\frac{2\times10^4}{10^9} \times \frac{B_c}{10^3} \approx 24$ bacteria in this area during the whole incubation cycle.

E. coli can propel themselves with 35 times their length per second (Chattopadhyay et al. 2006). Because of the random bacteria orientation, half of the bacteria would be propelling angled downward to the nanopillars, and for restrained calculation, the propelling speed was set to 20 µm/s. The propelling will result in $20 \times 12 \approx 240$ interactions with the nanopillar surface per second. During the incubation time of one hour, 8.6×10^5 nanopillar interactions would occur.

221 dead bacteria per 100×100 µm^2 field of view after the one-hour incubation cycle was the highest death count obtained in this study. By applying the two approaches of calculating the nanopillar interactions mentioned above, the liquidation efficiency is between $L_e = \frac{221}{5000} = 4\%$ for the calculation assuming settled bacteria and $L_{ea} = \frac{221}{8.6\times10^5} = 0.026\%$ for self-propelling bacteria. The maximum number of nanopillar-attached bacteria per 100×100 µm^2 field was 311, so even assuming that all attached living bacteria will die does not significantly affect the liquidation efficiency.

Various possibilities and combinations exist for estimating the number of bacteria interacting with the nanopillars. The number of bacteria in the proximity of the nanopillar surface is at least one order of magnitude higher than the number of killed bacteria.

We propose to interpret the low percentage of killed bacteria as an expression of an adherence impediment that hinders the bacteria from attaching to the surface (see "Nanopillar attachments in context of bacteria concentration" section). As the introduction described, the overstretching mechanism is the BM adhesion along the sides of the nanopillars that overstretches the BM area between the nanopillars. We suggest accepting the overstretching mechanism as the main antibacterial effect because of the adherence impediment and the quiescent testing situation (Román-Kustas et al. 2020).

Stacking of bacteria

The sample for the SEM micrograph Fig. 8 was prepared by drying an incubated wing specimen with dry air. One can see that the area covered by adhered bacteria is not exposing any nanopillars (Fig. 8). Bacteria attaching to the bacteria-covered surface will have no interactions with the nanopillars and yield typical survival ratios like in a non-nanopillar scenario. This study did not look directly into this issue. The protocols needed to clean the wing surfaces, ultrasonication bath in distilled water for 10 min, from bacteria debris indicate that the dead bacteria are rigidly attached to the surface (Bürger 2022; van Nieuwenhoven 2022). As the nanopillar surface gets polluted with debris, this will result in a loss of efficiency of the nanopillar surface.

Fig. 8 SEM micrograph of a *K. scutellaris* wing surface, dried with compressed-dry-air, after one-hour incubation. No rinsing was done. This resulted in a high concentration of *E. coli* bacteria forced to the nanopillar surface. The nanopillar surface was covered with bacteria. The bacteria above the dead surface bound bacteria will not be exposed to the nanopillar surface
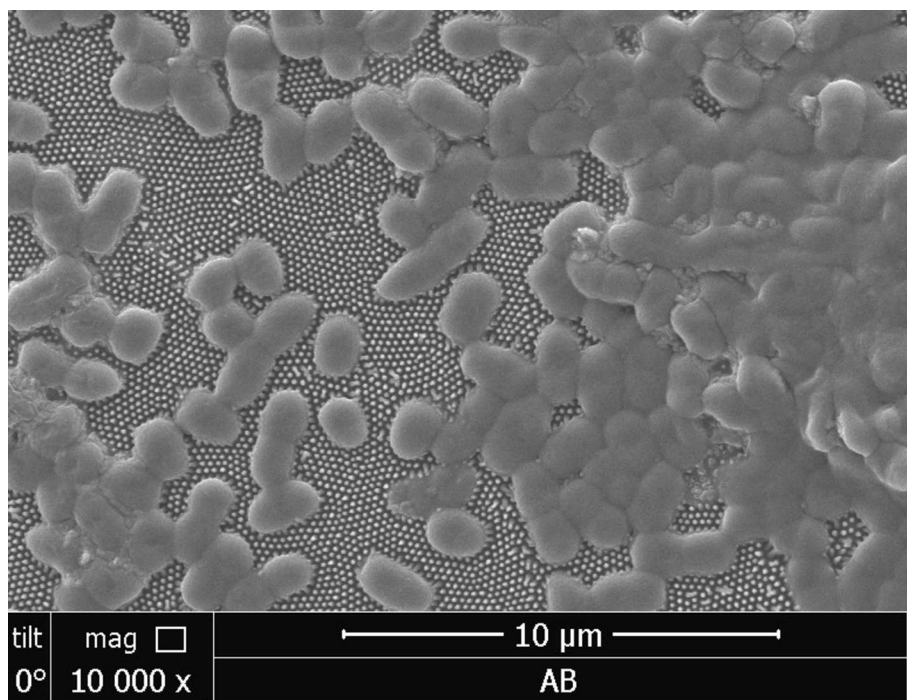
Summary and conclusions

The superhydrophobicity of the cicada wings enables self-cleaning and antifouling properties. Nature does not disclose whether the nanostructures on the wings of cicadas are intended to rupture bacteria.

The wings of the cicada species *A. cingulata* and *K. scutellaris* show nanopillar structures, and we could present their topology and antibacterial properties. Nanoscale precise wing surface replicas were produced using 4 °C cooled PVS replication procedures (Bürger 2022; van Nieuwenhoven 2022).

The testing procedures for the antibacterial properties have various variants and parameters. In concordance with other studies (Senevirathne et al. 2021; Hawi et al. 2022), it is proposed that these procedures should be harmonized to yield comparable results from different studies.

The results indicate adherence impediment that hinders the bacteria from attaching to the surface. We hypothesize that the superhydrophobicity of the nanopillar surface is responsible for the low attachment rate.

The bacteria that overcome the adherence impediment and attach to the nanopillar surface are destroyed by over-stretching the BM because of the BM adhesion along the sides of the nanopillars.

There is a tradeoff on nanostructured surfaces between hydrophobicity & self-cleaning mechanisms and antibacterial efficiency. This tradeoff must be considered when utilising biomimetic nanostructured surfaces in medical appliances. Considering the high concentration of bacteria used in the tests, compared to the lower one potentially occurring on insect wings in Nature, stacking bacteria on top of debris is unlikely to appear regularly in a natural environment. Therefore, stacking and its related problems are improbable evolutionary selection criteria during the evolution of the nanopillar surfaces.

We recommend that further studies look deeper into the overall efficiency of nanopillar surfaces as mechanical bactericides.

Supplementary information

The datasets generated during and/or analysed during the current study are available from the corresponding author on reasonable request.

Declarations

Conflict of interest The authors declare that they have no known competing financial interests or personal relationships that could have appeared to influence the work reported in this paper.

References

Bandara CD, Singh S, Afara IO, Wolff A, Tesfamichael T, Ostrikov K, Oloyede A (2017) Bactericidal effects of natural nanotopography of dragonfly wing on *Escherichia coli*. ACS Appl Mater Interfaces 9(8):6746–6760. https://doi.org/10.1021/acsami.6b13666

Baracchi D, Baciadonna L (2020) Insect sentience and the rise of a new inclusive ethics. Anim Sentience 5(29):18. https://doi.org/10.51291/2377-7478.1604

Bauer N et al (2021) A.Z.O.O.O.—A ZIMMER OF ONE'S OWN a phantastic journey into nanostructures. https://doi.org/10.13140/RG.2.2.18085.17123

Bertani G (1951) Studies on lysogenesis I. J Bacteriol 62(3):293–300. https://doi.org/10.1128/jb.62.3.293-300.1951

Buchanan RE (1918) Life phases in a bacterial culture. J Infect Dis 23(2):109–125. https://doi.org/10.1086/infdis/23.2.109

Bürger AML (2022) Surface analytics of bactericidal cicada wing nanopillars and development of a biomimetic nanoimprinting approach for functional replication. Master's thesis, Institute of Applied Physics, TU Wien, Vienna, Austria. https://doi.org/10.34726/hss.2022.90809

Chattopadhyay S, Moldovan R, Yeung C, Wu XL (2006) Swimming efficiency of bacterium *Escherichia coli*. Proc Natl Acad Sci 103(37):13712–13717. https://doi.org/10.1073/pnas.0602043103

Ciancio G, Pollack A, Taupier MA, Block NL, Irvin GL (1988) Measurement of cell-cycle phase-specific cell death using Hoechst 33342 and propidium iodide: preservation by ethanol fixation. J Histochem Cytochem 36(9):1147–1152. https://doi.org/10.1177/36.9.2457047

Hall B, Kirit HA, Nandipati A, Barlow M (2013) Growth rates made easy. Mol Biol Evol 31:232–238. https://doi.org/10.1093/molbev/mst187

Hasan J, Webb HK, Truong VK, Pogodin S, Baulin VA, Watson GS, Watson JA, Crawford RJ, Ivanova EP (2012) Selective bactericidal activity of nanopatterned superhydrophobic cicada psaltoda claripennis wing surfaces. Appl Microbiol Biotechnol 97(20):9257–9262. https://doi.org/10.1007/s00253-012-4628-5

Hawi S, Goel S, Kumar V, Pearce O, Ayre WN, Ivanova EP (2022) Critical review of nanopillar-based mechanobactericidal systems. ACS Appl Nano Mater 5(1):1–17. https://doi.org/10.1021/acsanm.1c03045

Huang E, Skoufis A, Denning T, Qi J, Dagastine R, Tabor R, Berry J (2021) OpenDrop: open-source software for pendant drop

tensiometry contact angle measurements. J Open Source Softw 6(58):2604. https://doi.org/10.21105/joss.02604

Ivanova EP, Hasan J, Webb HK, Truong VK, Watson GS, Watson JA, Baulin VA, Pogodin S, Wang JY, Tobin MJ, Löbbe C, Crawford RJ (2012) Natural bactericidal surfaces: mechanical rupture of *Pseudomonas aeruginosa* cells by cicada wings. Small 8(16):2489–2494. https://doi.org/10.1002/smll.201200528

Ivanova EP, Nguyen SH, Webb HK, Hasan J, Truong VK, Lamb RN, Duan X, Tobin MJ, Mahon PJ, Crawford RJ (2013a) Molecular organization of the nanoscale surface structures of the dragonfly *Hemianax papuensis* wing epicuticle. PLoS ONE 8(7):67893. https://doi.org/10.1371/journal.pone.0067893

Ivanova EP, Hasan J, Webb HK, Gervinskas G, Juodkazis S, Truong VK, Wu AHF, Lamb RN, Baulin VA, Watson GS, Watson JA, Mainwaring DE, Crawford RJ (2013b) Bactericidal activity of black silicon. Nat Commun 4(1):2838. https://doi.org/10.1038/ncomms3838

Ivanova EP, Nguyen SH, Guo Y, Baulin VA, Webb HK, Truong VK, Wandiyanto JV, Garvey CJ, Mahon PJ, Mainwaring DE, Crawford RJ (2017) Bactericidal activity of self-assembled palmitic and stearic fatty acid crystals on highly ordered pyrolytic graphite. Acta Biomater 59:148–157. https://doi.org/10.1016/j.actbio.2017.07.004

Kelleher SM, Habimana O, Lawler J, Reilly BO, Daniels S, Casey E, Cowley A (2015) Cicada wing surface topography: an investigation into the bactericidal properties of nanostructural features. ACS Appl Mater Interfaces 8(24):14966–14974. https://doi.org/10.1021/acsami.5b08309

Koch K, Schulte AJ, Fischer A, Gorb SN, Barthlott W (2008) A fast, precise and low-cost replication technique for nano- and high-aspect-ratio structures of biological and artificial surfaces. Bioinspiration Biomim 3(4):046002. https://doi.org/10.1088/1748-3182/3/4/046002

Mangels JI, Cox ME, Lindberg LH (1984) Methanol fixation an alternative to heat fixation of smears before staining. Diagn Microbiol Infect Dis 2(2):129–137. https://doi.org/10.1016/0732-8893(84)90008-7

Michalska M, Divan R, Noirot P, Laible PD (2021) Antimicrobial properties of nanostructured surfaces—demonstrating the need for a standard testing methodology. Nanoscale 13(41):17603–17614. https://doi.org/10.1039/d1nr02953c

Pogodin S, Hasan J, Baulin VA, Webb HK, Truong VK, Nguyen THP, Boshkovikj V, Fluke CJ, Watson GS, Watson JA, Crawford RJ, Ivanova EP (2013) Biophysical model of bacterial cell interactions with nanopatterned cicada wing surfaces. Biophys J 104(4):835–840. https://doi.org/10.1016/j.bpj.2012.12.046

Román-Kustas J, Hoffman JB, Reed JH, Gonsalves AE, Oh J, Li L, Hong S, Jo KD, Dana CE, Miljkovic N, Cropek DM, Alleyne M (2020) Molecular and topographical organization: influence on cicada wing wettability and bactericidal properties. Adv Mater Interfaces 7(10):2000112. https://doi.org/10.1002/admi.202000112

Sambrook J, Russell DW (2001) Molecular cloning—a laboratory manual. CSHL Press, Cold Spring Harbour

Schindelin J, Arganda-Carreras I, Frise E, Kaynig V, Longair M, Pietzsch T, Preibisch S, Rueden C, Saalfeld S, Schmid B, Tinevez J-Y, White DJ, Hartenstein V, Eliceiri K, Tomancak P, Cardona A (2012) Fiji: an open-source platform for biological-image analysis. Nat Methods 9(7):676–682. https://doi.org/10.1038/nmeth.2019

Scientific TF (2021) BestProtocols: viability staining protocol for flow cytometry. https://www.thermofisher.com/at/en/home/references/protocols/cell-and-tissue-analysis/protocols/viability-staining-flow-cytometry.html

Scientific TF (2021) Invitrogen™ Hoechst 33258 manual. https://www.thermofisher.com/document-connect/document-connect.html?

مدينة الملك عبدالعزيز
KACST للعلوم والتقنية ∑ Springer

url=https%3A%2F%2Fassets.thermofisher.com%2FTFS-Assets%2FLSG%2Fmanuals%2Fmp21486.pdf

Senevirathne SWMAI, Hasan J, Mathew A, Woodruff M, Yarlagadda PKDV (2021) Bactericidal efficiency of micro- and nanostructured surfaces: a critical perspective. RSC Adv 11(3):1883–1900. https://doi.org/10.1039/d0ra08878a

Tripathy A, Sen P, Su B, Briscoe WH (2017) Natural and bioinspired nanostructured bactericidal surfaces. Adv Colloid Interface Sci 248:85–104. https://doi.org/10.1016/j.cis.2017.07.030

Valiei A, Lin N, McKay G, Nguyen D, Moraes C, Hill RJ, Tufenkji N (2022) Surface wettability is a key feature in the mechano-bactericidal activity of nanopillars. ACS Appl Mater Interfaces 14(24):27564–27574. https://doi.org/10.1021/acsami.2c03258

van Nieuwenhoven RW (2022) Mechanical bactericide by biomimetics of the nanopillars on insect wings. Master's thesis, Institute of Applied Physics, TU Wien, Vienna, Austria. https://doi.org/10.34726/hss.2022.99685

Zhang X, Wang Y, Guo J, Yu Y, Li Y, Liu C (2015) Comparing two functions for optical density and cell numbers in bacterial exponential growth phase. J Pure Appl Microbiol 9:299–305

Zhang X, Zhang G, Chai M, Yao X, Chen W, Chu PK (2021) Synergistic antibacterial activity of physical-chemical multi-mechanism by TiO2 nanorod arrays for safe biofilm eradication on implant. Bioact Mater 6(1):12–25. https://doi.org/10.1016/j.bioactmat.2020.07.017

Zobl S (2018) Strukturfarben im Brennpunkt der Bionik Zwischen Kunst und Naturwissenschaften. Springer, Wiesbaden. https://doi.org/10.1007/978-3-658-20803-5